

Final Draft
of the original manuscript:

Vaidya, M.V.; Horstmann, M.; Venzke, V.; Petrovski, B.; Kocak, M.;
Kocik, R.; Tempus, G.:

**Structure-property investigations on a laser beam welded
dissimilar joint of aluminium AA6056 and titanium Ti6Al4V for
aeronautical applications, Part I: Local gradients in
microstructure, hardness and strength**

In: Materialwissenschaft und Werkstofftechnik (2009) Wiley

DOI: 10.1002/mawe.200900366

Structure-property investigations on a laser beam welded dissimilar joint of aluminium AA6056 and titanium Ti6Al4V for aeronautical applications

Part I: Local gradients in microstructure, hardness and strength

**Untersuchungen zu Struktureigenschaften von Laserstrahlgeschweißten
Mischverbindungen aus Aluminium AA6056 und Titan Ti6Al4V für
Anwendungen in der Luftfahrt**

Teil I: Lokale Gradienten in Mikrostruktur, Härte und Festigkeit

**W. V. Vaidya¹, M. Horstmann¹, V. Venzke¹, B. Petrovski¹, M. Koçak¹,
R. Kocik² and G. Tempus²**

¹GKSS Research Centre Geesthacht,
Institute of Materials Research,
Materials Mechanics,
Max-Planck-Strasse 1,
D-21502 Geesthacht,
Germany

²AIRBUS Deutschland GmbH,
Metal Technology,
Airbus-Allee 1,
D-28199 Bremen,
Germany

*Corresponding author
e-mail: waman.vaidya@gkss.de
Tel.: 0049 4152 872600
Fax.: 0049 4152 872534

Abstract

Sheets of AA6056 and Ti6Al4V were butt-joined by inserting the Ti-sheet into the profiled Al-sheet and by melting the Al-alloy alone using a split beam Nd:YAG laser. To study microstructural effects on properties, the Al-alloy was used in two tempers; T4 followed by post weld heat treatment T6, and in T6 followed by a defined duration of natural ageing at room temperature. As a basic step for fatigue and fracture investigations, local gradients in properties of this dissimilar joint are investigated using microscopy, hardness and tensile tests. Possible sites, from which fracture may initiate, have been then identified. All property changes are found to confine to the aluminium side. An intermetallic layer, although very thin, is found to form on the interface. The changeovers, firstly between the fusion zone and the heat affected zone and secondly between the heat affected zone and the base material, are found to be associated with changes in microstructure, hardness and strength. These are identified as the possible critical sites in addition to the interface.

Keywords: Aluminium alloy AA6056, Dissimilar weld, Hardness gradient, Laser beam welding, Microstructural variations, Property gradients, Tensile strength, Titanium alloy Ti6Al4V

Zusammenfassung

Durch eine spezielle Stossvorbereitung wurden laserstrahlgeschweißter Mischverbindungen aus den Blechwerkstoffen AA6056 und Ti6Al4V hergestellt und zwar ohne die Verwendung von Zusatzwerkstoffen. Die große Differenz der Schmelztemperaturen erlaubt das selektive Erschmelzen des Aluminiumwerkstoffs, der wiederum den Titanwerkstoff benetzt, so dass es zur Ausbildung einer mechanisch-stabilen und tragfähigen Verbindung kommt. Die Al-Legierung wurde in den Wärmebehandlungszuständen T4 und T6 verschweißt, um den mikrostrukturellen Einfluss auf die Eigenschaften der Verbindungen untersuchen zu können. Die Prozessfolgen sahen vor, dass beim Schweißen im Zustand T4 eine Warmauslagerung, beim Schweißen im Zustand T6 eine Kaltauslagerung definierter Dauer folgte. Die Charakterisierung lokaler Eigenschaftsgradienten hinsichtlich Gefüge, Mikrohärte und Festigkeit waren grundlegend für die Untersuchungen zum Ermüdungsrißausbreitungs- und Bruchverhalten der Mischerbindungen. Dabei wurden mögliche Bereiche, von denen Bruchversagen ausgehen könnte, identifiziert. Es hat sich gezeigt, dass die Eigenschaftsänderungen fast ausschließlich auf die Aluminiumseite beschränkt blieben. An der Grenzfläche zwischen Ti6Al4V und AA6056 wurde zudem eine schmale intermetallische Reaktionsschicht nachgewiesen. Diese lokalen Eigenschaftsänderungen im Gefüge, in der Härte und Festigkeit auf der Al-Seite sowie der intermetallische Phasensaum in Verbindung mit geometrischen Unterschieden sind im Rahmen der Untersuchungen als mögliche kritische Bereiche identifiziert worden.

Schlüsselworte: Aluminiumlegierung AA6056, Mischverbindung, Härtegradient, Laserstrahlschweißen, Gefügeänderungen, Eigenschaftsgradienten, Zugfestigkeit, Titanlegierung Ti6Al4V

1 Introduction

Use of welded integral structures [1] in airframes has been considered as a means for weight and cost reduction, and has already been realised by laser beam welding for skin-stringer panels [2,3]. One of the next targets is the dissimilar weld for the seat track [2,3] (shown in Fig. 1 to follow) for further weight saving and economy, since a specific material can be chosen for a specific local requirement. However, dissimilar welds are a metallurgical challenge [4]. Local gradients in microstructure, chemistry and properties become inherent and need to be accounted for in design. Moreover, when a non-ferrous partner is involved, intermetallic phases formed tend to be brittle [4] and consequently properties of the weld are impaired. Residual stresses [5] at the interface and in the partners may complicate the matter further.

With weight *alone* as the criterion, three base metals become interesting on the density basis; magnesium, aluminium and titanium. Magnesium is, however, yet to find acceptance for wide aerospace applications and so only Al- and Ti-alloys become relevant for dissimilar joints. Some physical properties collected from the literature [6] are shown in Table 1. It becomes clear that there are more differences than similarities and the properties are not in favour of fusion welding. Imaizumi [7] has assessed the weldability of aluminium to other partners in terms of electron beam welding. On a scale “no problem” to “impossible” he evaluates the dissimilar weld of aluminium and titanium as impossible. According to Sun and Ion [8] this situation is somewhat optimistic for laser beam welding on a scale “excellent” to “poor”, namely better than poor. Constructional modifications in the joint configuration coupled with melting of aluminium [9] or titanium [10] alone seem also not so successful, neither by electron beam weld [9] nor by laser beam welding [10], due to formation of intermetallics, cracking and low strength, particularly for alloys [9], or due to cracks and microporosity [10]. Thus, the use of fusion welding techniques seems to be difficult.

In contrast, non-fusion bonding appears to provide crack-free welds. By aluminizing titanium Jiangwei et al. [11] could diffusion bond pure titanium and pure aluminium. The weld had different intermetallics formed on the Ti-side but *not* on the Al-side. Explosive welding [12] is found to provide high strength, thermally stable and intermetallic-free joints for AA6061-Ti6Al4V laminates. However, thick sections or complex geometries may be a limitation. By friction welding satisfactory joints of pure Ti-AA5083 have been produced by Fuji et al. [13] using high pressure and short friction

time. In that case tensile failure is found to occur on the side of AA5083 (and not at the interface) and the interface is also found to be free from intermetallics. Use of cylindrical part is, however, a limitation. For parts involving sheets, friction stir welding can be an alternative. Okamura and Aota [14] have modified the friction stir welding process by inserting the pin towards the softer partner. Thereby, instead of the conventional stirring, plastic flow occurs in the softer partner, and bonding takes place by diffusion and by formation of a very thin alloy layer ($\leq 1 \mu\text{m}$) built on the harder partner. With such a process, steel-AA6XXX welds have been produced successfully [14-16]. The tensile fracture is found to occur in the weld zone (and not at the interface) and the fatigue lifetime to decrease by about 30 % in the high cycle regime [15]. The alloy layer and the intermetallic phase can indeed be kept very thin ($\leq 0.25 \mu\text{m}$) [16]. Fabrication of similar Ti6Al4V friction stir welded joints has been achieved only recently [17] but dissimilar sheet joints with Ti6Al4V have not yet been fabricated. Thus, although friction stir welding is promising, it is still under development.

Thus, it seems that at present there is no welding technique available on an industrial scale which can be applied to sheets of Al- and Ti-alloys. Laser beam welding is possible [8] but formation of intermetallics can become a limitation. Nonetheless, Schubert et al. [18] could show that by melting only aluminium the width of intermetallic can be restricted during laser beam welding and acceptable dissimilar joints for AA6XXX-steel can be produced. They demonstrated [19] this technique also on a two-meter long tailored blank. In a similar way AA6XXX-Ti6Al4V joints were produced by improving the technique and the welding parameters further [20-23]. Apparently, the technique of melting aluminium alone has now found a widespread resonance in the literature for laser beam welding of dissimilar joints involving Al-alloys [24].

We investigated such dissimilar weld sheets. The essential features [2,3,23] of the process in the present context are shown in Figs. 1a,b. The configuration is a butt-joint. The Al-alloy rib has a U-profile at the top, in which the Ti6Al4V sheet is inserted, Fig. 1a. By using a split beam laser from both sides only the Al-alloy is melted. The peak temperature is high ($< 1000^\circ\text{C}$) but not that high either to melt Ti6Al4V or to induce substantial solid state transformation in it. The molten aluminium wets Ti6Al4V, flows under the surface tension and the gravity, and yields a watertight joint, Fig. 1b. Since the laser is operated in the heat conduction mode (and not in the keyhole mode), loss of elements through evaporation does not occur in the Al-alloy. Thus, welding can be carried out even without a filler wire. The section shown in Fig. 1c is cut from a one-

meter long demonstrator and underlines the process applicability on the industrial scale. A typical coupon used in this investigation is shown later in Fig. 2.

The focus of this paper is on the structure-property relationship of the dissimilar joint and that too from a scientific (and not necessarily an industrial) viewpoint. Here (in Part I), local gradients in basic properties such as microstructure, hardness and strength are investigated and possible critical sites that may initiate failure are identified. These are usually the sites having non-uniform microstructure and undergo non-favourable plastic deformation. With this background fatigue crack propagation and fracture at these sites are investigated in Part II of this paper to follow.

In the following, the terminology “welding” [25] has been retained, since at least one partner was melted (and thus it is not considered as brazing). The partners are also referred to synonymously by the respective side, e.g., AA6056 as the Al-side. Moreover, specimens from the laboratory coupons (and not the component in Fig. 1c) have been tested.

2 Experimental procedure

Sheets of the precipitation hardenable AlMgSiCu type alloy, AA6056 (uniform thickness 2 mm) and Ti6Al4V (thickness 1.8 mm; mill annealed) were welded to coupons as shown in Figs. 1a,b using a split beam 4 kW Nd:YAG laser in the heat conduction mode at BIAS in Bremen, Germany, without using filler wire. The coupon had the dimensions 330 x 94 mm². To study the effect of starting microstructure on properties two tempers were selected for AA6056:

- welding in T4 followed by artificial ageing T6 (190 °C-4h/air); denoted also as “T4/T6” or “T4 followed by post weld heat treatment T6”, and
- welding in T6 and naturally aged (at least for 7 weeks) without any further artificial ageing; denoted also as “T6” without a special reference to the natural ageing.

Usually, the “start” and the “end” parts may be associated with inhomogeneous heat distribution during welding. To exclude such a possibility a region exhibiting constancy in the welding process and the temperature field was selected for specimen extraction. This region was then defined as testing region. For both welds the welding parameters were the same. In coupons welded in T6 the constancy of hardness was reached after 7 weeks of natural ageing. In contrast, the T4/T6 coupons, being

artificially aged, had not such a time restriction and could be tested immediately. A typical coupon is shown in Fig. 2. Specimens were extracted by electric discharge machining and tested after a minimum of 7 weeks time interval after welding.

Microstructure was investigated by optical metallography and scanning electron microscopy (SEM) using energy dispersive X-ray (EDX) analysis for local chemical gradients. Microhardness profile across the weld was obtained using an automated Vickers hardness testing machine at 0.2 kp (= 1.961 N) load and at an indentation interval of 0.3 mm. Each hardness traverse had more than about 150 indentations. Tensile tests were carried out on full-width strips 20 x 94 mm² using a laser extensometer and simultaneously a commercial image analysis system [26] to capture the instantaneous deformation pattern under the load. Such macro-tensile specimens provide global but not local information comparable to that obtained by microhardness. For that sake thin micro-flat tensile specimens having a thickness of 0.5 mm and reduced gauge section of 9 x 1.5 mm² were used. Such a specimen and the testing facility have been developed at GKSS [27]. Being relatively uncommon, an example of such a specimen is shown in Fig. 3 with a cut-off section (20 x 60 mm²) of a macro-tensile specimen for comparison.

3 Results and discussion

3.1 Visual observations

The coupons were within the testing region free from cracks and other defects such as undercuts, blowholes or spatter, which indicates a stable LBW process. The excess aluminium hump on titanium was also uniform on both sides. Occasionally, small isolated pores or chains of small pores (≤ 0.2 mm) were observed in X-ray radiography on the Al-side. Such pores can have their origin in gaseous impurity pick-up, in particular that of hydrogen [28]. In the present case it is also likely that pores have formed due to a gap during insertion of Ti6Al4V sheet and air entrapped in it (see Figs. 1a,b for the weld configuration).

The most evident imperfection was the distortion of the coupon. Welds, in general, are inherently prone for distortion which in turn is usually a result of residual stresses [5] induced. A feasibility investigation by energy dispersive synchrotron X-ray diffraction was supplemented by finite element analysis and the following trend has

emerged. On the Al-side residual stresses were mainly tensile in nature and decreased with the distance away from the interface. This is attributed to the melting and the solidification which occurs only on the Al-side and causes bending. At the interface there was a sharp changeover [5] in the residual stress pattern. On the Ti-side the stresses were compressive adjacent to the interface and changed to tensile away from the interface. Compressive stresses are induced due to the pressure exerted by the solidified aluminium and tensile stresses result probably due to expansion caused by the heat stagnation, since titanium has a low thermal conductivity (Table 1). Further attempts are being undertaken for residual stress measurements and should quantify the stress pattern described. In the context of testing, once the specimens were cut from the coupon, the remanent bending in specimens was substantially decreased due to the decrease and the redistribution of residual stresses.

3.2 Microstructural variations

That the Ti-side remained mostly unaffected was also confirmed by microstructural investigation. The major changes were confined to the Al-side, irrespective in which temper the joint was obtained, and are shown in Figs. 4 and 5. Two major zones were evident:

- the (initial) fusion zone extending up to about 3 mm from the interface and
- the (primary) heat affected zone extending up to about 7 mm from the interface.

Later (in Fig. 8), another zone (secondary, up to ca. 23 mm) is also reported but the primary heat affected zone is found to be more influential for properties.

The fusion zone encompassed the Ti-side by forming curves on either side (visible in macrographs) and had nearly equiaxed grains with broadened grain boundaries (due to segregation). Towards the end of the fusion zone a transition zone was formed where the elongated grain started to appear and their form tended to become comparable to that of the base material. At the end of the fusion zone and the beginning of the heat affected zone grain boundary liquation was observed up to a length of about 4 grains. Grain boundary liquation is typical [29-33] to butt joints of laser beam welded 6XXX Al-alloys that are welded by the keyhole mode. In the present case energy input was not that high due to the heat conduction mode. Nonetheless, the grain boundary liquation seems to be a general phenomenon in the fusion welded Al-alloys and deserves attention due to the segregation and the locking-up of the solute (in grain boundaries).

At the beginning of the heat affected zone there was a thin region which exhibited recrystallised equiaxed grains. Otherwise, in the adjacent region polygonised network was observed (visible in Fig. 4). This is clearly an effect resulting from heat conduction through the Al-side and indicates softening of material. The initial grain shape (partially recrystallised and pan caked) was, however, retained in the heat affected zone. The basic microstructural features were comparable in both types of welds, with the difference that in the T6-weld coarsening of precipitates in grain interior and precipitate free zones at the grain boundary were evident.

The major criterion for the quality of the joint is the formation and the width of the intermetallic [4]. If its formation cannot be avoided, at least its width should be kept to a minimum possible. The interface between the Al- and Ti-side could be observed at a sufficiently high magnification and resolution only by SEM and in the back scattered electron (BSE) mode, and is shown in Fig. 6. A layer with the saw tooth profile was found to form on all sides on the interface. Its morphology varied between threads and plates (see Fig. 7 also). On an average the width was about $1.8 \pm 0.3 \mu\text{m}$, and was nearly the same in both starting tempers and did not change after post weld heat treatment. Therefore, the layer had been formed during welding. The only difference was that after post weld heat treatment the space in between the saw teeth appeared to some extent filled-in, probably with secondary precipitates formed during the artificial ageing.

The essential message from the literature (e.g., [4]) is that the chemical nature of the layer at the interface is decisive for its properties. We used EDX analysis for the local chemical analysis as shown in Fig. 7. The chemical gradient was found to be very steep and indicates a local inter-diffusion within a very small reaction zone during melting. With the crossover of K_{α} lines as the measure, the zone width was found to be less than $2.7 \mu\text{m}$. The chemical analysis of three adjacent areas is given in Table 2. At the interface the composition is nearer to TiAl_3 . That the chemical gradient is steep (e.g., [13]) and that on the Al-side TiAl_3 forms (e.g., [34]) is in agreement with the literature. Compared to Ti_3Al and TiAl which have a compositional range, TiAl_3 is a line compound and unfortunately brittle.

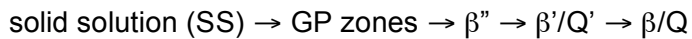
Imazumi [7] urges to use a fusion method that avoids the formation of brittle intermetallics. Insofar his conclusion “compounds of aluminium and titanium are *unbrittle* and have little effect on the joint strength” possibly does not refer to TiAl_3 .

Following the work at BIAS [18-23] and AIRBUS [2-3] the message should read that if a brittle compound cannot be avoided, it should at least be very thin. This was achieved presently (Figs. 6-7).

3.3 Hardness gradient

Microhardness is a good indicator to find out weak sites. The present data are shown in Fig. 8. As for microstructure, the major changes were confined to the Al-side and had similarities in that the hardness variations were found also at about 3 mm (fusion zone) and 7 mm (heat affected zone) from the interface. In contrast, at the interface hardness increased sharply and remained nearly constant on the Ti-side. In T4/T6, the post weld heat treatment T6 improved the hardness in the fusion zone partially but that in the heat affected zone was improved nearly completely to that of the base material level (Fig. 8a). On the other hand, the dip in hardness at about 7 mm still remained. Effect of welding on loss of hardness in the fusion zone and the heat affected zone was evident in laser beam welding T6 (Fig. 8b) which was not heat treated again, except for the natural ageing. Here, after the fusion zone, hardness increased slightly (due to the natural ageing) but dropped again at about 7 mm. After this dip the trend on the Al-side was found to be comparable in both welds. The hardness in the Al-base material reached a constant value nearly after about 23 mm from the interface. This latter part between 7 mm and 23 mm is an extended (i.e. secondary) heat affected zone and an effect related to heat conduction on the Al-side.

To understand the hardness trend, the precipitation in AA6XXX alloys [35,36] needs to be considered. These are basically AlMgSi alloys and are hardened by metastable variants of β , Mg_2Si (stable phase; plate-shaped). During ageing, clustering of atoms is followed by the formation of needle-shaped Guinier-Preston (GP) zones. The major hardening precipitate is coherent β'' (metastable; needles) and overages into semi-coherent β' (metastable; needles/rods) and finally into incoherent β . When Cu is added, as in AA6056 [35] an additional phase Q, $Al_5Cu_2Mg_8Si_6$ (stable phase; plate-shaped) and its semi-coherent variant Q' (metastable; laths/rods) are formed while β'' , β' and β may be partly suppressed [36]. The precipitation sequence [35,36] can be described as:



and is sensitive to time delay in quenching [37] and to variations [38] in batch composition and in tempering temperature. Moreover, Q' can have compositional and

structural similarities to β'' (and β') [35], and also different variants [37]. All these factors make the precipitation sequence complex. In AA6056 the major hardening constituents [31,32,35,38] are GP zones in T4 and β'' (β'/Q') in T6.

From the literature [31,32,35,38-40] and assuming that below the liquidus the overall precipitation process is similar in friction stir welding and laser beam welding, a schematics of the correlation between hardness variations and precipitates ("Sato et al. Diagram" [41]) is attempted in Fig. 9 for the Al-side.

When welded in T6, the loss of hardness in the fusion zone is associated with dissolution of the hardening precipitates and in the heat affected zone additionally with overaging of precipitates, although there is a partial recovery in these regions (up 7 mm) through GP zones after natural ageing. It is recalled here that this was the reason why these specimens were tested after 7 weeks and after reaching constancy in hardness. In T4/T6, the hardness recovery in the fusion zone was partial due to non-availability (or limited availability) of the solute, probably because the solute, although not lost, was tied as β/Q . On the other hand, in the heat affected zone (up to 7 mm) the hardness recovery was nearly complete in the sense that hardness level nearly that of the base material was reached after the post weld heat treatment T6 (Figs. 8a, 9a). Thus, the heat affected zone seems to have undergone solution annealing during welding but re-precipitation during the post weld heat treatment.

Mg is the major constituent of the hardening precipitates of precursors of Mg_2Si and is likely to be lost through vaporisation during laser beam welding. Our on-going work on precipitation in bulk studied by small-angle neutron scattering (SANS) has shown that in the *keyhole-mode* fabricated laser beam welded butt-joints of AA6056 the loss of Mg in the fusion zone can be nearly 50 %. This observation is basically in agreement with that by Fabregue et al. [32] by transmission electron microscopy (TEM). The practical consequence of loss of Mg is a partial recovery of hardness in the fusion zone after the post weld heat treatment [42]. Presently, when the laser beam welded joint is fabricated in the *heat conduction mode*, the hardness is also recovered only partially (Fig. 8a). However, here Mg is tied (Fig. 9a) but not lost through vaporisation and, therefore, this mode seems to be advantageous. It also follows that if the weld T6 in Fig. 8b was re-tempered to T6 again, its hardness in the fusion zone should have been improved similar to that in Fig. 8a, since Mg is not lost.

In the base material (after ca. 23 mm) the maximum hardness level was reached, which indicates a stable precipitate state. Between 3 mm (fusion zone) and 23 mm the hardness varied substantially and the least hardness was found to be in the heat affected zone (at 7 mm). This is attributed to heat flow and in turn to overageing and coarsening of precipitates. Once the stable phases form (β/Q ; β'/Q'), the solute is tied and is no more available for hardening. Therefore, the hardness dip at 7 mm persists even after the post weld heat treatment T6 and has nearly the same value in both the welds. From 7 mm to 23 mm hardness increases again (Figs. 8-9), since the extent of thermal effects (overageing) during laser beam welding decreases with the increase in the distance from the interface. The practical consequence is that the soft zones tend to form at 3 mm and 7 mm from the interface, and shall have the consequence of strength loss and strength undermatching. In turn, these sites are likely to be the preferential sites for deformation and fracture.

3.4 Tensile properties

From hardness values it was expected that the Al-side should exhibit low strength. By using macro-specimens with markers for different gauge lengths as shown in Fig. 10 regional and global information was obtained. The tensile curves are shown in Fig. 11 along with the typical strain distribution at various stress levels, and the data in Table 3. Since major plastic deformation occurred on the Al-side, the stress levels were calculated by assuming uniform thickness of the Al-side for the mixed zone as well as for the global region.

The joint in T6 was more ductile due to overaging than that in T4/T6 which being peak-hardened had higher strength, Fig. 11. This difference is also seen as colour difference in the deformation pattern images. The Al-side was due to strength undermatching prone for plastic deformation. As expected from the hardness gradient (Figs. 8-9) the site "7 mm" turned out to be weakest site right from the beginning of loading, and led to fracture. Therefore, despite differences in microstructure and microhardness, the maximum stress level reached was comparable in both joints (≈ 235 MPa). Irrespective in which temper the joint was welded, the Ti-side and also to some extent the mixed zone (being thickened by the hump) exhibited mainly elastic behavior. As mentioned, the hump (being non-uniform in thickness) was not considered for stress calculations. The local thickening has in fact protected the weld by reducing the stress level. There are variations also in Young's modulus depending on the temper

(Table 3). Thus, by changing the heat treatment it should be possible to control the deformation behaviour of this dissimilar weld.

The impression that the region “mixed zone” in Fig. 11 is exhibiting low deformation and is thus brittle is a result of local constraint and gauge length used [42]. Thus, when the plastic deformation is very local and non-uniform, and the gauge length is long, the elongation tends to be gauge length dependent (Figs. 10-11; Table 3). For additional confirmation, micro-flat tensile specimens (shown in Fig. 3) were extracted from different locations perpendicular to the weld and tested, as shown in Fig. 12. The data are given in Table 4. The essential difference between these two types of specimens is that in contrast to the macro specimen the micro-flat specimen is free from constraint. It must be mentioned that the region “mixed zone” in Figs. 10-11 and Fig. 12 is not necessarily the same.

Micro-flat tensile specimens from the Ti6Al4V-side exhibited a slight difference in strength, which should be considered as scatter (and not an effect resulting from the post weld heat treatment to T6), Fig. 12. On the contrary, specimens from the AA6056-side exhibited a nearly identical behaviour, which is to be expected since the base material in both type of joints was peak-aged to T6 and the specimens, being extracted away from the heat affected zone, were also not affected by the heat flow. The micro-flat tensile specimens from the mixed zone fractured either at “3 mm” or at “7 mm” site but not at the interface. When broken at “7 mm” site, the fracture strain was lower than that at “3 mm” site. It is for this reason that the tensile curves of the mixed zone specimens differ. In both cases the joint is thus deformable.

Since the specimens fractured on the Al-side (and not exactly at the interface), the strength of the interface cannot be obtained. Nonetheless, the data show that the joint is sound and should have a good tensile strength, at least of 220 MPa, and be still higher at the interface since the latter remained intact. Thus, although $TiAl_3$ formed (Figs. 6-7, Table 2) and should have been brittle, it does not limit the deformability of the joint in the present case. We expect that the tensile strength of the interface shall be higher than that of the Al-side and, therefore, the interface shall exhibit elastic deformation.

3.5 Additional remarks

This investigation was a basic step to identify critical sites for further fatigue and fracture investigations. The term “critical” sounds catastrophic but being a common practice, is used also here and should be understood as “preferential”. Usually it is expected that sites having non-uniform microstructure shall undergo non-favourable plastic deformation and lead to fracture. On this basis, the sites identified as critical are shown in Fig. 13 as a summary of this investigation. The “interface” should have high strength but low ductility. In contrast, the site “7 mm” should exhibit low strength but high ductility, and the site “3 mm” an intermediate behavior and the fracture should be on the Al-side. Thus, the site “7 mm”, due to its low strength, becomes critical under static tensile loading (Fig. 11, Table 3). On the other hand, since this site exhibits substantial deformation, it may not be that critical in the context of fracture toughness. Since parameters in favour of fracture resistance may not be the same for the resistance to fatigue crack propagation, further investigations are undertaken on the notched specimens and the results reported in Part II of this paper to follow.

4 Conclusions

1. The dissimilar laser beam welds of AA6056 and Ti6Al4V, fabricated by inserting Ti-sheet into the profiled Al-sheet and melting AA6056 alone, were found to be sound and mechanically stable in the context of testing.
2. In the joints, gradients in microstructure, chemical composition, hardness and strength were observed. That such gradients are very steep is in agreement with the literature. All changes were confined to the side of AA6056. In contrast, Ti6Al4V remained practically unaffected.
3. At the joint interface an intermetallic layer near to the composition $TiAl_3$ was found. Its width was, however, very small ($1.8 \pm 0.3 \mu m$). Tensile fracture was observed on the Al-side and not at the interface. Insofar, the layer, although formed, did not impair the deformation.
4. Soft zones are found to form at microstructural changeovers between the initial fusion zone and the heat affected zone (3 mm from the interface) and between the heat affected zone and the base material (7 mm from the interface). A secondary heat affected zone is found to extend on the Al-side (from 7 mm to 23 mm) and is attributed to the heat flow and to the formation of different precursors of stable precipitates which tie-up the solute and, hence, restrict the hardness recovery.

5. In contrast to the heat affected zone, hardness could be recovered partially in the fusion zone for specimens welded in T4 and given post weld heat treatment T6. On the other hand, those welded in T6 exhibited softening. Thus, although gradients in properties cannot be avoided, the sequence, welding in T4 followed by artificial ageing T6, seems favourable to increase the strength.
6. Fracture of the macro specimens under tensile loading occurred at the site "7 mm" from interface (heat affected zone) due to plastic strain concentration in this soft zone. A minimum in hardness was also observed at this site. The site "3 mm" (in fusion zone) was characterised by a changeover from dendritic to wrought microstructure and exhibited a slightly higher microhardness than that at the site "7 mm". Micro-flat tensile specimens showed that the weld was not brittle.

Acknowledgements

This work was funded by AIRBUS and additionally by GKSS Research Centre. We gratefully acknowledge this financial support.

Literature

1. K.-H. Rendigs: Aluminium structures used in aerospace- status and prospects, *Mater. Sci. Forum*, **1997**, 242, pp. 11-24.
2. R. Kocik, S. Kaschel, M. Kreimeyer, J. Schumacher and F. Vollertsen: Development of a new joining technology for hybrid metal aircraft structures, in *ICALEO 2004*, Proc. 23rd Int. Conf. on Application of Lasers and Electro-Optics 2004, San Francisco, California, USA, 04-07 Oct. 2004, Laser Institute of America (LIA) Congr. Proc., CD-ROM 597, LIA, Orlando, Florida, USA, **2004**.
3. R. Kocik, T. Vugrin, T. Seefeld: Laser beam welding in airframe structures, status and future applications, (in German), in 5. Laser-Anwendungforum, 13-14. Sept., 2006, Bremen, *Laserstrahlfügen: Prozesse, Systeme, Anwendungen, Trends*, (ed. F. Vollertsen und T. Seefeld), Strahltechnik, Band 28, Bremen, Germany, BIAS-Verlag, **2006**, pp. 15-26.
4. N. Bailey: Review of metallurgical problems in dissimilar metal welding, in *Welding Dissimilar Metals*, (ed. N. Bailey), The Welding Institute, Cambridge, Great Britain, 1986, pp. 1-6.
5. K. Bing, B. Eigenmann, B. Scholtes and E. Macherauch: Brazing residual stresses in components of different metallic materials, *Mater. Sci. Engng. A*, **1994**, A174, pp. 95-101.
6. C. M. Smithells (ed.): Metals Reference Book, 5th edition, Butterworths, London, England, **1976**.
7. S. Imaizumi: Welding of aluminium to dissimilar metals, *Weld. Int.*, **1996**, 10, pp. 593-604.
8. Z. Sun and J. C. Ion: Laser welding of dissimilar metal combinations, *J. Mater. Sci.*, **1995**, 30, pp. 4205-4214.
9. P. Skoda, J. Dupak and P. Michalicka: Creation of heterogeneous weld joints of titanium- and aluminium-based materials by electron beam welding, in Proc. Int. Welding Conf., Japan Slovak Welding Symp., Tatranske Matliare, Tatranska Lomnica, **1996**, paper 30, pp. 157-160.
10. M. Cabibbo, S. Marrone and E. Quadrini: Mechanical and microstructural characteristics of laser welded titanium-aluminium joints, *Weld. Int.*, **2005**, 19, pp. 125-129.
11. R. Jiangwei, L. Yajiang and F. Tao: Microstructure characteristics in the interface zone of Ti/Al diffusion bonding, *Mater. Lett.*, **2002**, 56, pp. 647-652.

12. E. S. Ege and O. T. Inal: Stability of interfaces in explosively-welded aluminium titanium laminates, *J. Mater. Sci. Lett.*, **2000**, 19, pp. 1533-1535.
13. A. Fuji, M. Kimura, T. H. North, K. Ameyama and M. Aki: mechanical properties of titanium-5083 aluminium alloy friction joints, *Mater. Sci. Technol.*, **1997**, 13, pp. 673-678.
14. H. Okamura and K. Aota: Joining of dissimilar materials with friction stir welding, *Weld. Int.*, **2004**, 18, pp. 852-860.
15. H. Uzun, C. Dalle Donne, A. Argagnotto, T. Ghidini and C. Gambaro: Friction stir welding of dissimilar Al 6013-T4 to X5CrNi18-10 stainless steel, *Mater. Design*, **2005**, 26, pp. 41-46.
16. W.-B. Lee, M. Schmuecker, U. A. Mercardo, G. Biallas and S.-B. Jung: Interfacial reaction in steel-aluminium joints made by friction stir welding, *Scr. Mater.*, **2006**, 55, pp. 355-358.
17. Y. Zhang, Y. S. Sato, H. Kokawa, S. H. C. Park and S. Hirano: Microstructural characteristics and mechanical properties of Ti-6Al-4V friction stir welds, *Mater. Sci. Engng. A*, **2008**, 485, pp. 448-455.
18. E. Schubert, I. Zerner and G. Sepold: New possibilities for joining by using high power diode lasers, in *ICALEO 98*, Proc. Int. Conf. on Laser Materials Processing 1998, Laser Institute of America (LIA), Congr. Proc., Vol. 85, LIA, Orlando, Florida, USA, **1998**, Section G, pp. 111-120.
19. E. Schubert, M. Klassen, I. Zerner, C. Walz and G. Sepold: Leight-weight structures produced by laser beam joining for future applications in automobile and aerospace industry, *J. Mater. Process. Technol.*, **2001**, 115, pp. 2-8.
20. F. Wagner, I. Zerner, M. Kreimeyer, T. Seefeld and G. Sepold: Characterization and properties of dissimilar metal combinations of Fe/Al and Ti/Al-sheet materials, in *ICALEO 2001*, Proc. 20th Int. Conf. on Applications of Lasers & Electro-Optics 2001, Laser Institute of America (LIA), Congr. Proc., CD-ROM, LIA, Orlando, Florida, USA, **2001**, pp. 365-374.
21. M. Kreimeyer, F. Wagner, I. Zerner and G. Sepold: Laser beam joining of aluminium with titanium with the use of an adapted working head, (in German), in *DVS-Berichte, Band 212*, Düsseldorf, Germany, DVS-Verlag, **2001**, pp. 93-98,
22. M. Kreimeyer, F. Wagner and F. Vollertsen: laser processing of aluminium-titanium-tailored blanks, *Opt. Laser. Engng.* **2005**, 43, pp. 1021-1035.
23. F. Wagner, M. Kreimeyer, R. Kocik and F. Vollertsen: Laser joining of aluminium to titanium with focus on aeronautical applications, in *PICALO 2006*, Proc. 2nd Int. Conf. on Applications of Lasers and Optics 2006, (ed. M. Brandt and E. Harvey),

Laser Institute of America (LIA), Congr. Proc. CD-ROM 401, LIA, Orlando, Florida, USA, **2006**, pp. 42-47.

24. S. Katayama: Laser welding of aluminium alloys and dissimilar metals, *Weld. Int.*, **2004**, 18, pp. 618-625.
25. S. P. Parker (ed.): *McGraw-Hill Dictionary of Scientific and Technical Terms*, 4th edition, McGraw-Hill Book Company, New York, USA, **1989**, 2056.
26. ARAMIS, Optical Deformation Analysis System (www.gom.com).
27. G. Cam, S. Riekehr and M. Koçak: Determination of mechanical properties of laser beam welded steel joints with microtensile specimens, IIW Doc. SC X-F-055-97, **1997**.
28. M. Mazur: Porosity in aluminium welds, *Weld. Int.*, **1992**, 36, pp. 929-931.
29. B.C. Meyer, E. Lectard and N. Serrano, E. Zschech, T. Hirsch and P. Mayr: Laser beam welding of Al-Mg-Si-Cu alloy 6013, (in German), *Härtereitechnische Mitteilung*, **1997**, 52, pp. 291-297.
30. R. Braun, C. Dalle Donne and G. Staniek: Laser beam welding and friction stir welding of 6013-T6 aluminium alloy sheet, *Mat.-wiss. u. Werkstofftech.*, **2000**, 31, pp. 1017-1026.
31. D. Fabregue and A. Deschamps: Microstructural study of laser welds-AS12 in relation with hot tearing, *Mater. Sci. Forum*, **2002**, 396-402, pp. 1567-1572.
32. D. Fabregue, A. Deschamps and M. Suery: Microstructure of butt laser joints of aluminium alloy 6056 sheets with an AS12 filler, *Mater. Sci. Technol.*, **2005**, 21, pp. 1329-1336.
33. W. V. Vaidya, K. Angamuthu, M. Koçak, R. Grube and J. Hackius: Strength and fatigue resistance of laser-MIG hybrid butt welds of an airframe aluminium alloy AA6013, *Welding in the World*, **2006**, 50, No. 11/12, pp. 88-97.
34. M. Sujata, S. Bhargava and S. Sangal: On the formation of TiAl₃ during reaction between solid Ti and liquid Al, *J. Mater. Sci. Lett.*, **1997**, 16, pp. 1175-1178.
35. M. Tanaka and T. Warner: Quantitative TEM study of hardening precipitates in 6XXX aluminium alloys, *La Revue de Métallurgie*, **2003**, 100, pp. 463-469.
36. H. S. Hasting, J. C. Walmsley, A. T. J. van Helvoort, C. D. Marioara, S. J. Andersen and R. Holmestad: Z-contrast imaging of arrangement of Cu in 6XXX series aluminium alloys, *Phil. Mag. Lett.*, **2006**, 86, pp. 589-597.
37. N. I. Kolobnev, L. B. Khokhlatova, S. V. Samokhvalov, A. A. Alekseev, S. V. Sbitneva, T. I. Tararaeva and V. I. Popov: Heat treatment effect on properties of Al-Mg-Si-Cu 1370 alloy, *Mater. Sci. Forum*, **2006**, 519-521, pp. 519-524.

38. F. Delmas, M. J. Casanove, P. Lours, A. Couret and A. Coujou: Quantitative TEM study of precipitation microstructure in aluminium alloy Al(MgSiCu) 6056T6, *Mater. Sci. Engng. A*, **2004**, 373, pp. 80-89.
39. C. Gallais, A. Simar, D. Fabregue, A. Denquin, G. Lapasset, B. de Meester, Y. Brechet and T. Pardoen: Multiscale analysis of the strength and ductility of AA6056 aluminium friction stir welds, *Metall. Mater. Trans. A*, **2007**, 38A, pp. 964-981.
40. M. Cabibbo, H. J. Mcqueen, E. Evangelista, S. Spigarelli, M. Di Paola and A. Falchero: Microstructure and mechanical property studies of AA6056 friction stir welded plate, *Mater. Sci. Engng. A*, **2007**, 460-461, pp. 86-94.
41. Y. S. Sato, H. Kokawa, M. Enomoto and S. Jogan: Microstructural evolution of 6063 aluminium during friction stir welding, *Metall. Mater. Trans. A*, **1999**, 30A, pp. 2429-2437.
42. W. V. Vaidya, M. Koçak, E. Seib, H. Assler and J. Hackius: Mechanical behavior of laser beam and friction stir welded aluminium alloys for airframes, *Welding in the World*, **2006**, 48, Special Issue No. 7, pp. 261-273.

Figure captions

Figure 1. Salient features of the laser beam welding process. The arrangement of sheets is shown schematically in a) and the dissimilar joint configuration fabricated by melting aluminium alone in b) (schematics after AIRBUS). The section in c) is a cut-away piece from a one-meter demonstrator for the airplane seat track.

Abbildung 1. Besondere Merkmale des Laserstrahlschweißprozesses. Die Anordnung der Bleche ist in a) schematisch dargestellt und die Herstellung der Mischverbindung, bei der nur das Aluminium aufgeschmolzen wird, in b) (schematische Darstellung nach AIRBUS). Der Ausschnitt in c) zeigt ein Segment einer zu Demonstrationszwecken hergestellten Sitzschiene.

Figure 2. A typical laser beam welded coupon showing the region, from which different types of specimens for testing were extracted (dimensions in mm).

Abbildung 2. Bereich der Laserstrahlschweißverbindung, aus dem Proben für die Untersuchungen herausgetrennt wurden (Abmessungen in mm).

Figure 3. Micro-flat tensile test specimen used for local properties. The flat macro-tensile specimen is shown for comparison. (For a better visibility of the micro-flat specimen the strip is shortened in length from 94 mm to 60 mm).

Abbildung 3. Mikroflachzugproben für die Untersuchung der lokalen Eigenschaften. Zum Vergleich ist die Makroflachzugprobe gegenübergestellt. (Zur besseren Sichtbarkeit der Mikroflachzugproben wurde die Streifenlänge von 94 mm auf 60 mm gekürzt).

Figure 4. Microstructural variations on the side of AA6056, laser beam welded in the T4 condition and post weld heat treated to T6 for peak-ageing. The frames on the macrograph show the locations where the micrographs in the lower row were taken.

Abbildung 4. Gefügeänderungen auf der AA6056-Seite, laserstrahlgeschweißt im Zustand T4 und anschließend warmausgelagert in den Zustand T6. Die Rahmen in den makroskopischen Darstellungen kennzeichnen die Bereiche, aus denen die Gefügedarstellungen stammen.

Figure 5. Microstructural variations on the side of AA6056, laser beam welded in the T6 condition and defined naturally aged. The frames on the macrograph show the locations where the micrographs in the lower row were taken.

Abbildung 5. Gefügeänderungen auf der AA6056-Seite, laserstrahlgeschweißt im Zustand T6 und definiert kaltausgelagert. Die Rahmen in den makroskopischen Darstellungen kennzeichnen die Bereiche, aus denen die Gefügedarstellungen stammen.

Figure 6. Formation of a phase seam in the reaction zone. Note that the maximum width of the phase seam is nearly the same, irrespective of the initial temper of AA6056 before the laser beam welding, (SEM back scattered electron image; see also Fig. 7).

Abbildung 6. Bildung eines Phasensaums an der Grenzfläche zwischen AA6056 und Ti6Al4V. Zu beachten ist, dass die maximale Breite des Phasensaums nahezu gleich ist und zwar unabhängig von dem AA6056-Zustand vor dem Laserstrahlschweißen (Materialkontrast, s. auch Abbildung 7).

Figure 7. Steep changeover in the chemical gradient at the interface in terms of the Ti- K_{α} and Al- K_{α} line traces corresponding to the location indicated by the scan line in a).

Abbildung 7. Steiler chemischer Gradient in Bezug auf die charakteristischen Ti- K_{α} - und Al- K_{α} -Röntgenlinien. Das Profil dieser Elemente wurde entlang der Linie in a) aufgezeichnet.

Figure 8. Partial recovery of the hardness after post weld heat treatment, a), and its loss when welded in the peak-aged condition, b). Note that the gradient in hardness is confined to the side of AA6056 only. The inset shows the location of the hardness traverse. Measured each from the interface, the fusion zone is extending up to about 3 mm, the primary heat affected zone up to 7 mm and the secondary up to 23 mm. Hardness thereafter is nearly the same in both type of welds.

Abbildung 8. Begrenzter Wiederanstieg der Härte infolge der Warmauslagerung auf T6 nach dem Laserstrahlschweißen in T4, a), und der Verlust an Härte, wenn im Zustand T6 laserstrahlgeschweißt wird, b). Der Härtegradient ist ausschließlich im

Bereich der Aluminiumlegierung AA6056 zu verzeichnen. Die eingezeichneten Linien zeigen schematisch die Lage der Härtemesslinien an. Die Schmelzzone in beiden Varianten hat, bezogen auf die Grenzfläche, eine Ausdehnung von etwa 3 mm, die primäre Wärmeeinflusszone eine Ausdehnung von 7 mm ab dem Interface und die sekundäre Wärmeeinflusszone eine Ausdehnung von 23 mm ab dem Interface.

Figure 9. A schematics of the correlation between hardness variation on the side of AA6056 and the state of precipitation in various regions in the present case. The extended heat affected zone is indicated by the arrowed dotted line. Hardness levels reached after solution annealing (SS: solid solution) and artificial ageing T4 and T6 are shown for comparison by gray horizontal lines. Diagram based on the presentation by Sato et al. [41] and the literature data on precipitates in AA6XXX alloys [31,32,35,38-40].

Abbildung 9. Eine schematische Darstellung des Zusammenhangs zwischen Härteänderung auf der AA6056-Seite und den Ausscheidungszuständen in den verschiedenen Gefügebereichen. Die ausgedehnte Wärmeeinflusszone ist durch die gestrichelte Linie angedeutet. Dem sind die Grundwerkstoff-Härteniveaus in den Zuständen Lösungsgeglüht, T4 und T6 gegenüber gestellt, erkennbar an den horizontalen grauen Linien. Grundlage für die Diagramme ist die Arbeit von Sato et al. [41] sowie Literaturdaten zu Ausscheidungszuständen in AA6XXX-Legierungen [31,32,35,38-40].

Figure 10. Gauge positions for the tensile data in the local and the global regions defined. The laser extensometer scans in the vertical direction, from the bottom to the top and measures the extension between the lower edges. The total global gauge length is 20 mm, sectioned in 5 mm each for the Al- and Ti-side and 10 mm for the mixed zone. The region “mixed zone” in Figs. 10-11 and Fig. 12 is not necessarily the same. Due to 3D-perspective the dimensions are distorted.

Abbildung 10. Festgelegte Positionen zur Erfassung von Zugversuchskenndaten. Mit dieser Anordnung war es möglich, die Festigkeit und Verformung sowohl lokal als auch global zu bestimmen. Die Messung erfolgte mit einem Laserextensometer in vertikaler Richtung von oben nach unten. Gemessen wurden relativen Längenänderung zwischen den unteren Kanten der jeweiligen weißen Streifen auf der Probe. Die globale Länge betrug 20 mm, aufgeteilt in 5 mm für die Al- und Ti-Seite und 10 mm für

die gemischte Zone. Diese gemischte Zone ist nicht unbedingt die gleiche wie in Abb. 10-11 und Abb. 12. Infolge der perspektivischen Darstellung sind die Dimensionen im Bild verzerrt.

Figure 11. Tensile curves in the local regions along with the pairs “front face and cross section” of the instantaneous optical deformation pattern at a given stress level. The macrograph shows the fracture location which is at 7 mm from the interface on the side of AA6056 in both type of welds. (The region “mixed zone” in Figs. 10-11 and Fig. 12 is not necessarily the same).

Abbildung 11. Globale und lokale Spannung-Dehnung-Kurven. In den jeweiligen Verformungsbildern sind sowohl die Front- als auch die Querschnittseite der Mischverbindung dargestellt. Den makroskopischen Abbildungen ist zu entnehmen, dass unabhängig von der Prozessfolge Bruchversagen in einem Abstand von etwa 7 mm von der Grenzfläche auf der AA6056-Seite der jeweiligen Mischverbindung eintrat. (Die gemischte Zone ist nicht unbedingt die gleiche wie in Abb. 10-11 und Abb. 12).

Figure 12. Relative locations of the micro-flat tensile specimens in the base materials and in the mixed zone, a), and the corresponding tensile curves, b). Thin lines correspond to the data from the laser beam weld in the T4 condition of AA6056 followed by post weld heat treatment T6, and the thick lines to that welded in the T6 condition and defined naturally aged. For the latter a typical fracture of the mixed zone specimen is shown in the inset, and is on the side of AA6056 while the interface is intact. (The region “mixed zone” in Figs. 10-11 and Fig. 12 is not necessarily the same).

Abbildung 12. Die Entnahmeorte für die Mikroflachzugproben sind in a) gezeigt, die zugehörigen Spannung-Dehnung-Kurven in b). Die dünnen Linien gehören zu den Mikroflachzugproben aus der T4 laserstrahlgeschweißten und nachfolgend in den Zustand T6 warmausgelagerten Verbindung, die dicken Linien zu den Mikroflachzugproben aus der Verbindung, die im Zustand T6 laserstrahlgeschweißt und anschließend definiert kaltausgelagert wurde. Das eingefügte Bild zeigt eine gebrochene Mikroflachzugprobe aus der gemischten Zone. Der Bruch trat auf der AA6056-Seite ein. (Die gemischte Zone ist nicht unbedingt die gleiche wie in Abb. 10-11 und Abb. 12)

Figure 13. Relative location of sites shown schematically on the dissimilar weld, at which notable changes in microstructure, hardness, strength and deformation behaviour were observed. (Vertical lines denote these sites which were to be notched for fatigue crack propagation and fracture testing. The continuation of the heat affected zone as a secondary zone shown in Figs. 8-9 is indicated by the arrow).

Abbildung 13. Die verschiedenen Bereiche auf der Al-Seite, in denen hinsichtlich Festigkeit, Härte und Gefüge Änderungen beobachtet wurden, sind durch vertikale Linien gekennzeichnet. (Diese entsprechen Positionen für Ermüdungsrißausbreitungs- und Bruchmechanikversuche, in welche Kerben und Risse künstlich eingebracht werden. Die Fortsetzung der primären Wärmeeinflusszone als sekundäre Zone, gezeigt in Abb. 8-9, ist mit dem Pfeil angedeutet).

Table 1: Differences in some properties of pure titanium and pure aluminium (literature data [6]).

Tabelle 1: Unterschiede in den Eigenschaften zwischen Reintitan und Reinaluminium (Literaturdaten [6]).

Property	Titanium	Aluminium
Atomic weight	47.90	26.98
Crystal structure	CPH	FCC
Density (kgm^{-3})	4500	2700
Melting temperature (K)	1940	933
Thermal conductivity ($\text{Wm}^{-1}\text{K}^{-1}$)	21.6	238
Coefficient of thermal expansion (10^{-6}K^{-1})	8.9	23.5
Mean specific heat ($\text{Jkg}^{-1}\text{K}^{-1}$)	528	917
Terminal solid solubility at 723 K	6.5 wt. % Al	ca. 0.2 wt. % Ti
First terminal intermetallic	$\text{Ti}_3\text{Al}^{\text{a)}}$	$\text{TiAl}_3^{\text{a)}}$
Young's modulus, E (GPa)	120.2	70.6

^{a)} Ti_3Al has a compositional range and is deformable (i.e., non-brittle). As against, TiAl_3 is a line compound, without a comparable compositional range, and is brittle.

Table 2: Quantitative chemical analysis of areas within the interface and the base materials AA6056 and Ti6Al4V by energy dispersive X-rays, both in wt. % and at. %.

Tabelle 2: Chemische Zusammensetzung des intermetallischen Phasensaums und der Grundwerkstoffe AA6056 sowie Ti6Al4V, bestimmt mit dem EDX-Verfahren (Angaben in Gew. % und At. %).

Element	Interface		Ti6Al4V		AA6056	
	wt. %	at. %	wt. %	at. %	wt. %	at. %
Mg	0.19	0.25			0.40	0.45
Al	64.84	75.73	5.87	9.99	98.59	98.90
Si	2.29	2.68			0.20	0.20
Ti	31.14	20.47	88.99	85.37	*	*
V	1.41	0.87	5.15	4.64		

*Traces of Ti were found in AA6056 due to secondary excitation and this effect is an artefact.

Table 3: Tensile properties of the local and the global regions as defined in Fig. 10 and the curves shown in Fig. 11, obtained on macro specimens. (The region “mixed zone” in Figs. 10-12 is not necessarily the same).

Tabelle 3: Globale und lokale Kennwerte aus dem Zugversuch gemäß der Anordnung (s. Abb. 10 und 11). (Die gemischte Zone in Abb. 10-12 ist nicht unbedingt die gleiche).

Region	LBW in T4 and PWHT T6				LBW in T6			
	E (GPa)	R _{p0.2} (MPa)	R _m (MPa)	A (%)	E (GPa)	R _{p0.2} (MPa)	R _m (MPa)	A (%)
Ti-side	115	-	n.a.	0.29	77	-	n.a.	0.29
Mixed zone	79	-	n.a.	0.34	53	195	n.a.	0.5
Al-side	77	145	235	11.1	45	130	235	14.6
Global	36	195	235	2.8	56	165	235	4.0

n.a.: not applicable. Since the specimens fracture at the “7 mm” site, the ultimate strength of all regions is masked by the strength of this site.

Table 4: Tensile properties of the base materials, Ti6Al4V (Ti-side) and AA6056 (Al-side), and the mixed zone as defined and shown in Fig. 12, obtained on micro-flat tensile specimens. (The region “mixed zone” in Figs. 10-12 is not necessarily the same).

Tabelle 4: Kenndaten aus dem Zugversuch an Mikroflachzugproben, welche aus den jeweiligen Grundwerkstoffen und aus der gemischte Zone entnommen wurden, wie in Abb. 12 dargestellt. (Die gemischte Zone in den Abb. 10-12 ist nicht unbedingt die gleiche).

Region	LBW in T4 and PWHT T6				LBW in T6			
	E (GPa)	R _{p0.2} (MPa)	R _m (MPa)	A (%)	E (GPa)	R _{p0.2} (MPa)	R _m (MPa)	A (%)
Ti-side	100	910	980	14.8	95	850	920	15.8
Al-side	65	325	375	8.1	60	330	380	8.0
Mixed zone	67	210	240	3.7	45	155	225	8.9

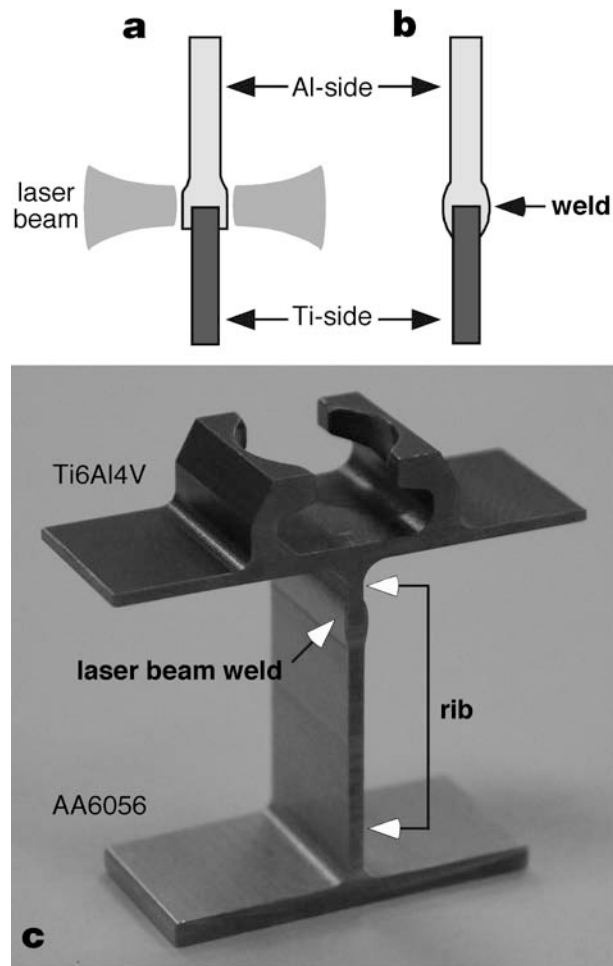


Figure 1. Salient features of the laser beam welding process. The arrangement of sheets is shown schematically in a) and the dissimilar joint configuration fabricated by melting aluminium alone in b) (schematics after AIRBUS). The section in c) is a cut-away piece from a one-meter demonstrator for the airplane seat track.

Abbildung 1. Besondere Merkmale des Laserstrahlschweißprozesses. Die Anordnung der Bleche ist in a) schematisch dargestellt und die Herstellung der Mischverbindung, bei der nur das Aluminium aufgeschmolzen wird, in b) (schematische Darstellung nach AIRBUS). Der Ausschnitt in c) zeigt ein Segment einer zu Demonstrationszwecken hergestellten Sitzschiene.

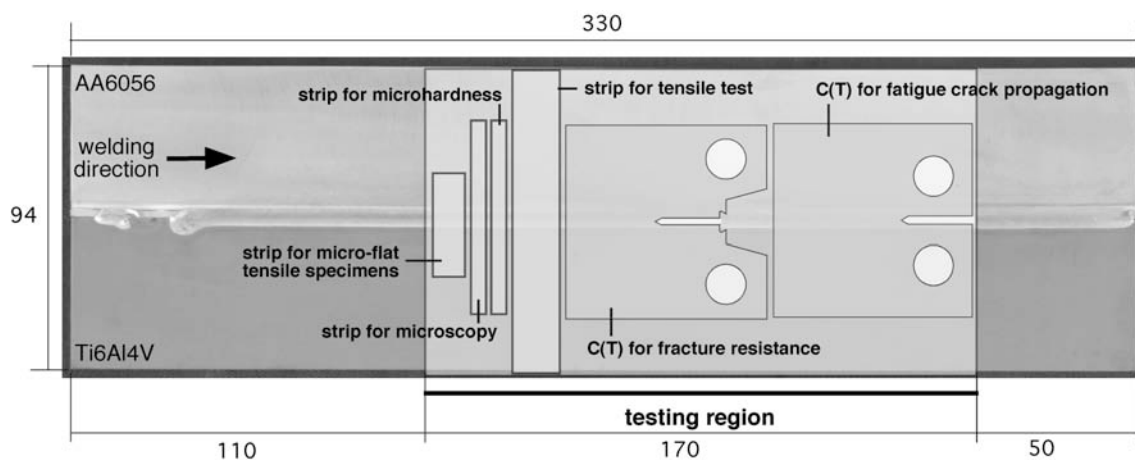


Figure 2. A typical laser beam welded coupon showing the region, from which different types of specimens for testing were extracted (dimensions in mm).

Abbildung 2. Bereich der Laserstrahlschweißverbindung, aus dem Proben für die Untersuchungen herausgetrennt wurden (Abmessungen in mm).

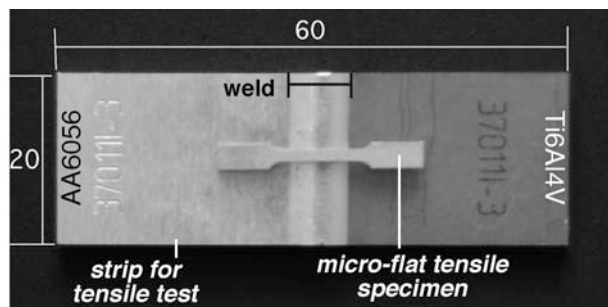


Figure 3. Micro-flat tensile test specimen used for local properties. The flat macro-tensile specimen is shown for comparison. (For a better visibility of the micro-flat specimen the strip is shortened in length from 94 mm to 60 mm).

Abbildung 3. Mikroflachzugproben für die Untersuchung der lokalen Eigenschaften. Zum Vergleich ist die Makroflachzugprobe gegenübergestellt. (Zur besseren Sichtbarkeit der Mikroflachzugproben wurde die Streifenlänge von 94 mm auf 60 mm gekürzt).

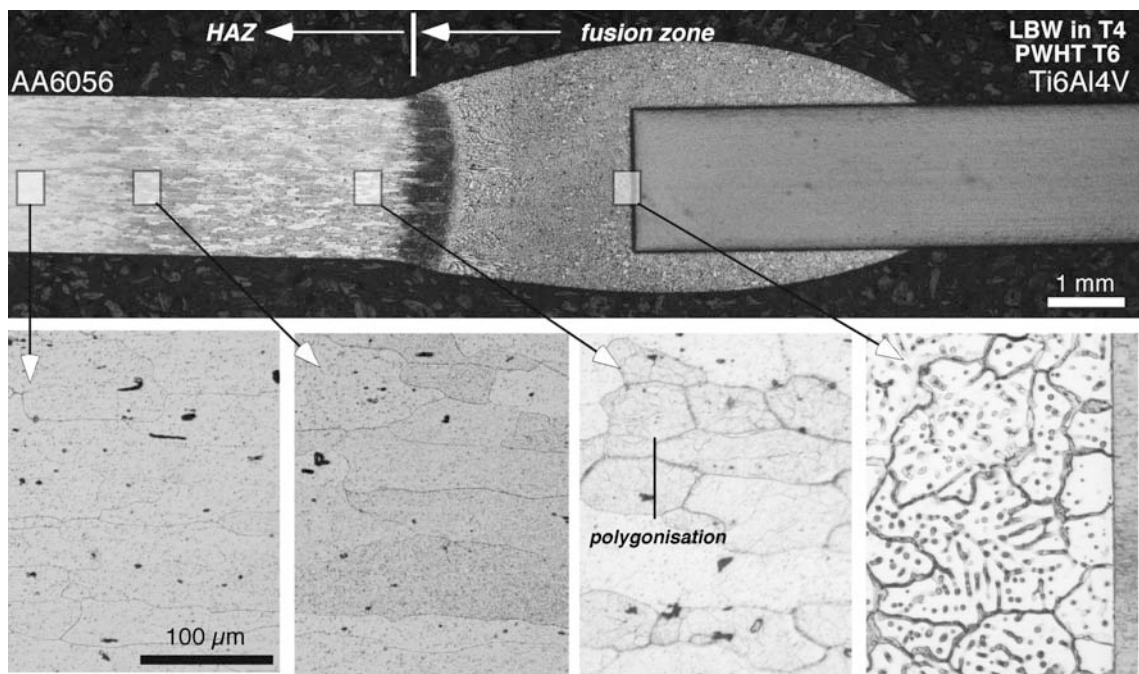


Figure 4. Microstructural variations on the side of AA6056, laser beam welded in the T4 condition and post weld heat treated to T6 for peak-ageing. The frames on the macrograph show the locations where the micrographs in the lower row were taken.

Abbildung 4. Gefügeänderungen auf der AA6056-Seite, laserstrahlgeschweißt im Zustand T4 und anschließend warmausgelagert in den Zustand T6. Die Rahmen in den makroskopischen Darstellungen kennzeichnen die Bereiche, aus denen die Gefügedarstellungen stammen.

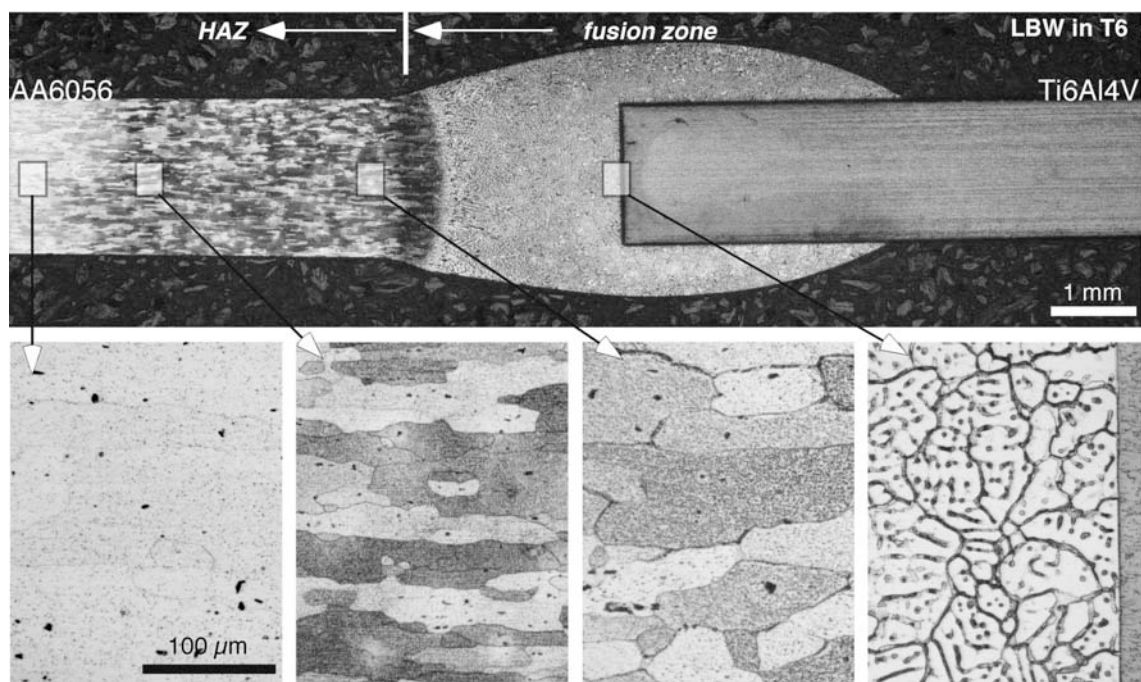


Figure 5. Microstructural variations on the side of AA6056, laser beam welded in the T6 condition and defined naturally aged. The frames on the macrograph show the locations where the micrographs in the lower row were taken.

Abbildung 5. Gefügeänderungen auf der AA6056-Seite, laserstrahlgeschweißt im Zustand T6 und definiert kaltausgelagert. Die Rahmen in den makroskopischen Darstellungen kennzeichnen die Bereiche, aus denen die Gefügedarstellungen stammen.

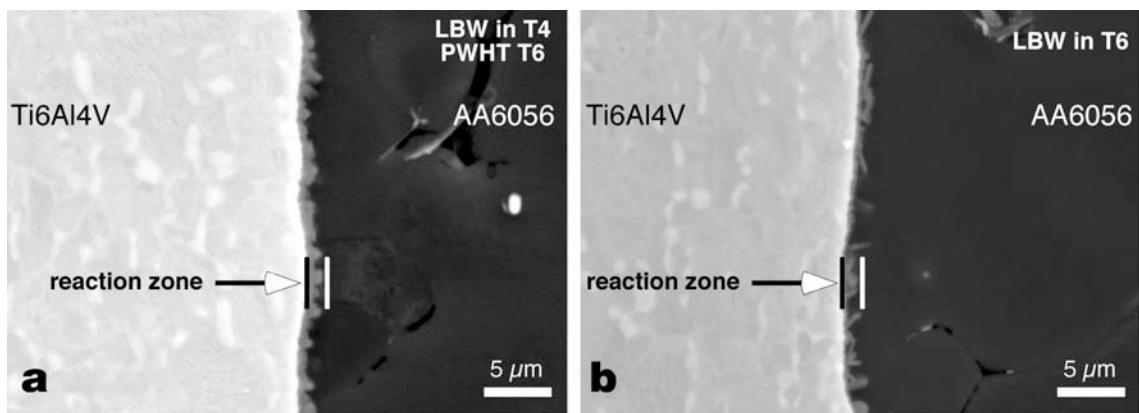


Figure 6. Formation of a phase seam in the reaction zone. Note that the maximum width of the phase seam is nearly the same, irrespective of the initial temper of AA6056 before the laser beam welding, (SEM back scattered electron image; see also Fig. 7).

Abbildung 6. Bildung eines Phasensaums an der Grenzfläche zwischen AA6056 und Ti6Al4V. Zu beachten ist, dass die maximale Breite des Phasensaums nahezu gleich ist und zwar unabhängig von dem AA6056-Zustand vor dem Laserstrahlschweißen (Materialkontrast, s. auch Abbildung 7).

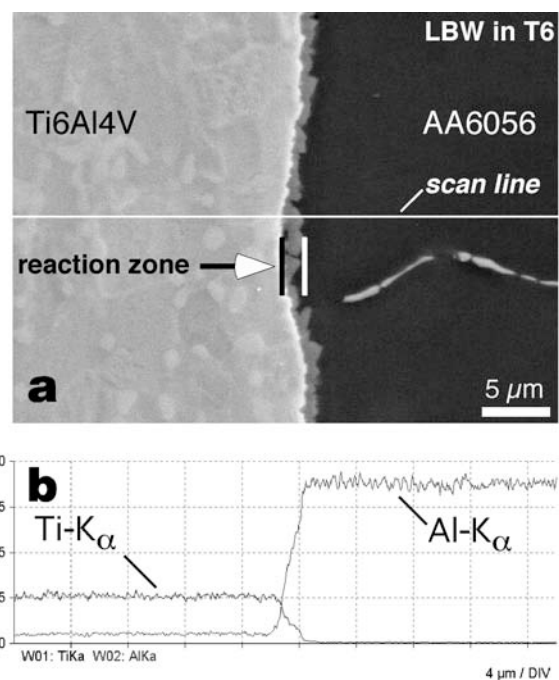


Figure 7. Steep changeover in the chemical gradient at the interface in terms of the $\text{Ti}-\text{K}_\alpha$ and $\text{Al}-\text{K}_\alpha$ line traces corresponding to the location indicated by the scan line in a).

Abbildung 7. Steiler chemischer Gradient in Bezug auf die charakteristischen $\text{Ti}-\text{K}_\alpha$ - und $\text{Al}-\text{K}_\alpha$ -Röntgenlinien. Das Profil dieser Elemente wurde entlang der Linie in a) aufgezeichnet.

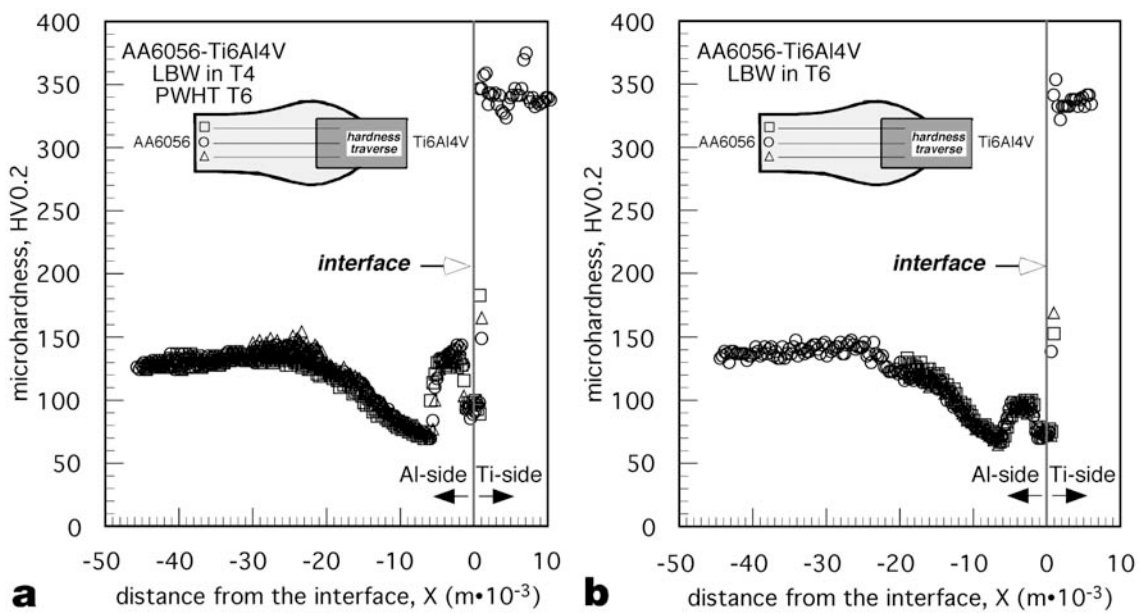


Figure 8. Partial recovery of the hardness after post weld heat treatment, a), and its loss when welded in the peak-aged condition, b). Note that the gradient in hardness is confined to the side of AA6056 only. The inset shows the location of the hardness traverse. Measured each from the interface, the fusion zone is extending up to about 3 mm, the primary heat affected zone up to 7 mm and the secondary up to 23 mm. Hardness thereafter is nearly the same in both type of welds.

Abbildung 8. Begrenzter Wiederanstieg der Härte infolge der Warmauslagerung auf T6 nach dem Laserstrahlschweißen in T4, a), und der Verlust an Härte, wenn im Zustand T6 laserstrahlgeschweißt wird, b). Der Härtegradient ist ausschließlich im Bereich der Aluminiumlegierung AA6056 zu verzeichnen. Die eingezeichneten Linien zeigen schematisch die Lage der Härtemesslinien an. Die Schmelzzone in beiden Varianten hat, bezogen auf die Grenzfläche, eine Ausdehnung von etwa 3 mm, die primäre Wärmeeinflusszone eine Ausdehnung von 7 mm ab dem Interface und die sekundäre Wärmeeinflusszone eine Ausdehnung von 23 mm ab dem Interface.

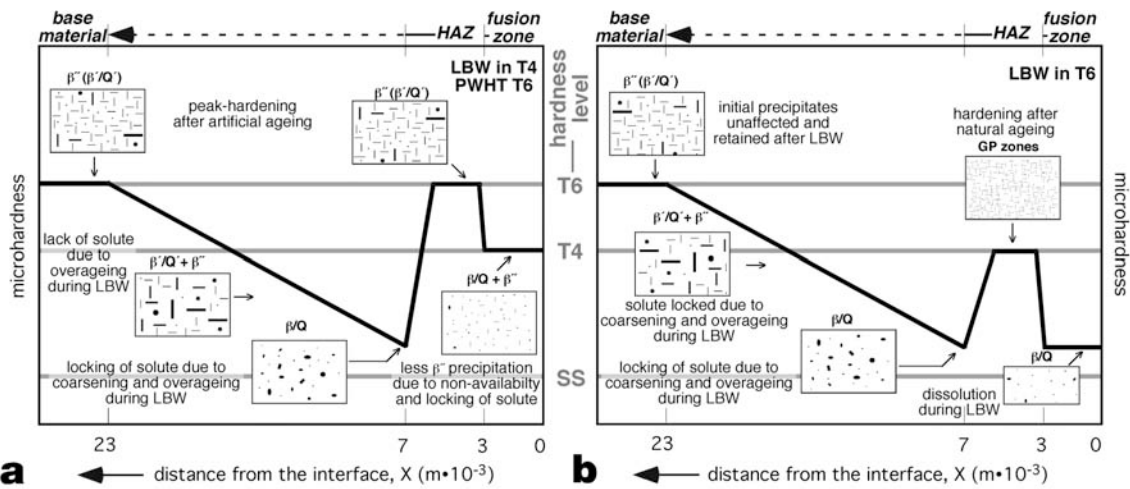


Figure 9. A schematics of the correlation between hardness variation on the side of AA6056 and the state of precipitation in various regions in the present case. The extended heat affected zone is indicated by the arrowed dotted line. Hardness levels reached after solution annealing (SS: solid solution) and artificial ageing T4 and T6 are shown for comparison by gray horizontal lines. Diagram based on the presentation by Sato et al. [41] and the literature data on precipitates in AA6XXX alloys [31,32,35,38-40].

Abbildung 9. Eine schematische Darstellung des Zusammenhangs zwischen Härteänderung auf der AA6056-Seite und den Ausscheidungszuständen in den verschiedenen Gefügebereichen. Die ausgedehnte Wärmeeinflusszone ist durch die gestrichelte Linie angedeutet. Dem sind die Grundwerkstoff-Härteniveaus in den Zuständen Lösungsgeglüht, T4 und T6 gegenüber gestellt, erkennbar an den horizontalen grauen Linien. Grundlage für die Diagramme ist die Arbeit von Sato et al. [41] sowie Literaturdaten zu Ausscheidungszuständen in AA6XXX-Legierungen [31,32,35,38-40].

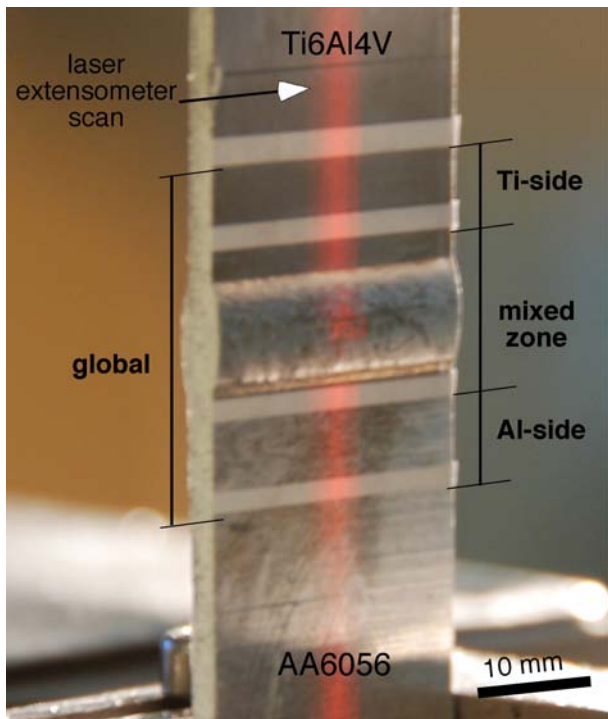


Figure 10. Gauge positions for the tensile data in the local and the global regions defined. The laser extensometer scans in the vertical direction, from the bottom to the top and measures the extension between the lower edges. The total global gauge length is 20 mm, sectioned in 5 mm each for the Al- and Ti-side and 10 mm for the mixed zone. The region “mixed zone” in Figs. 10-11 and Fig. 12 is not necessarily the same. Due to 3D-perspective the dimensions are distorted.

Abbildung 10. Festgelegte Positionen zur Erfassung von Zugversuchskenndaten. Mit dieser Anordnung war es möglich, die Festigkeit und Verformung sowohl lokal als auch global zu bestimmen. Die Messung erfolgte mit einem Laserextensometer in vertikaler Richtung von oben nach unten. Gemessen wurden relativen Längenänderung zwischen den unteren Kanten der jeweiligen weißen Streifen auf der Probe. Die globale Länge betrug 20 mm, aufgeteilt in 5 mm für die Al- und Ti-Seite und 10 mm für die gemischte Zone. Diese gemischte Zone ist nicht unbedingt die gleiche wie in Abb. 10-11 und Abb. 12. Infolge der perspektivischen Darstellung sind die Dimensionen im Bild verzerrt.

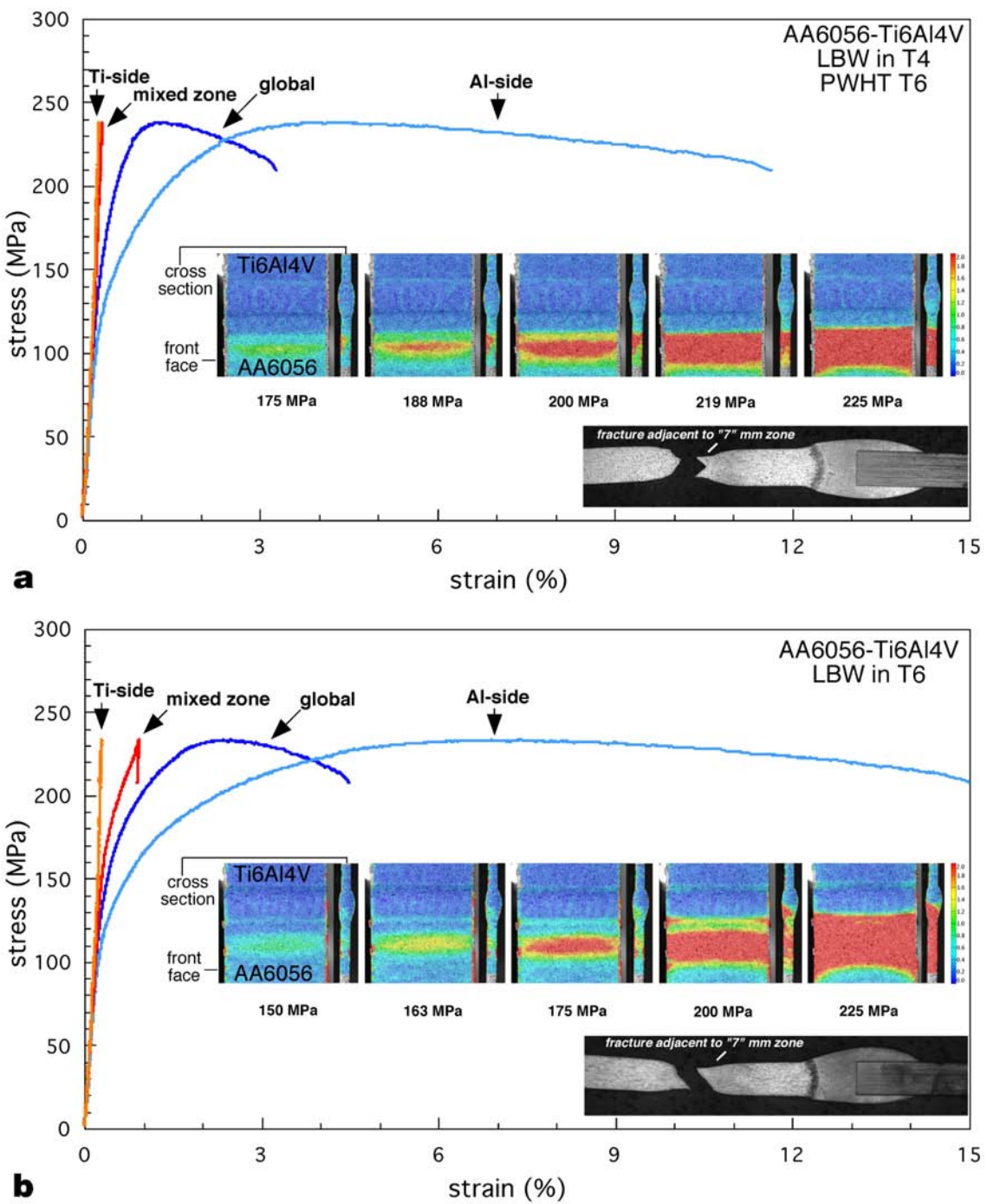


Figure 11. Tensile curves in the local regions along with the pairs “front face and cross section” of the instantaneous optical deformation pattern at a given stress level. The macrograph shows the fracture location which is at 7 mm from the interface on the side of AA6056 in both type of welds. (The region “mixed zone” in Figs. 10-11 and Fig. 12 is not necessarily the same).

Abbildung 11. Globale und lokale Spannung-Dehnung-Kurven. In den jeweiligen Verformungsbildern sind sowohl die Front- als auch die Querschnittseite der Mischverbindung dargestellt. Den makroskopischen Abbildungen ist zu entnehmen, dass unabhängig von der Prozessfolge Bruchversagen in einem Abstand von etwa 7 mm von der Grenzfläche auf der AA6056-Seite der jeweiligen Mischverbindung eintrat. (Die gemischte Zone ist nicht unbedingt die gleiche wie in Abb. 10-11 und Abb. 12).

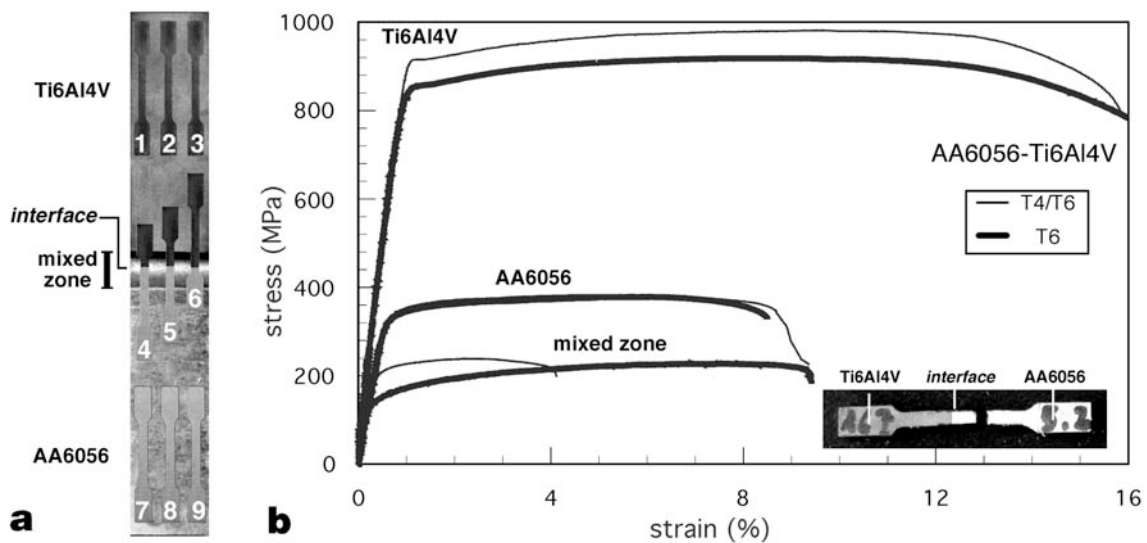


Figure 12. Relative locations of the micro-flat tensile specimens in the base materials and in the mixed zone, a), and the corresponding tensile curves, b). Thin lines correspond to the data from the laser beam weld in the T4 condition of AA6056 followed by post weld heat treatment T6, and the thick lines to that welded in the T6 condition and defined naturally aged. For the latter a typical fracture of the mixed zone specimen is shown in the inset, and is on the side of AA6056 while the interface is intact. (The region "mixed zone" in Figs. 10-11 and Fig. 12 is not necessarily the same).

Abbildung 12. Die Entnahmeorte für die Mikroflachzugproben sind in a) gezeigt, die zugehörigen Spannung-Dehnung-Kurven in b). Die dünnen Linien gehören zu den Mikroflachzugproben aus der T4 laserstrahlgeschweißten und nachfolgend in den Zustand T6 warmausgelagerten Verbindung, die dicken Linien zu den Mikroflachzugproben aus der Verbindung, die im Zustand T6 laserstrahlgeschweißt und anschließend definiert kaltausgelagert wurde. Das eingefügte Bild zeigt eine gebrochene Mikroflachzugprobe aus der gemischten Zone. Der Bruch trat auf der AA6056-Seite ein. (Die gemischte Zone ist nicht unbedingt die gleiche wie in Abb. 10-11 und Abb. 12)

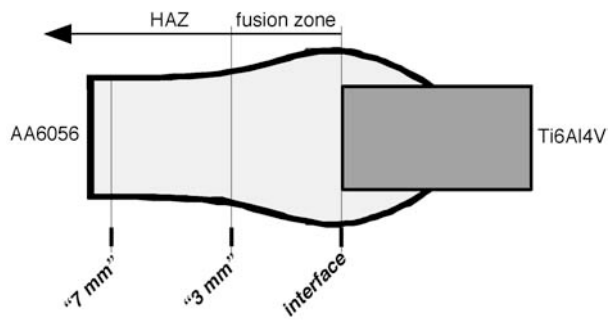


Figure 13. Relative location of sites shown schematically on the dissimilar weld, at which notable changes in microstructure, hardness, strength and deformation behaviour were observed. (Vertical lines denote these sites which were to be notched for fatigue crack propagation and fracture testing. The continuation of the heat affected zone as a secondary zone shown in Figs. 8-9 is indicated by the arrow).

Abbildung 13. Die verschiedenen Bereiche auf der Al-Seite, in denen hinsichtlich Festigkeit, Härte und Gefüge Änderungen beobachtet wurden, sind durch vertikale Linien gekennzeichnet. (Diese entsprechen Positionen für Ermüdungsrissausbreitungs- und Bruchmechanikversuche, in welche Kerben und Risse künstlich eingebracht werden. Die Fortsetzung der primären Wärmeeinflusszone als sekundäre Zone, gezeigt in Abb. 8-9, ist mit dem Pfeil angedeutet).